6

Advanced Vibro-Acoustic Techniques for Noise Control in Helicopters

Emiliano Mucchi[1], Elena Pierro[2] and Antonio Vecchio[3]
[1]*Engineering Department, University of Ferrara*
[2]*DIMeG, Politecnico di Bari*
[3]*ARTEMIS Joint Undertaking, Brussels*
[1,2]*Italy*
[3]*Belgium*

1. Introduction

Originally, aircraft noise was not much of an issue because of the overarching requirement of improving vehicle performance in critical operational conditions. For many years, the design of aircraft and helicopter has been challenged by the need to improve aeromechanical performance, leaving little rooms for considering additional design parameters such as noise, vibrations and passenger comfort. More recently, a paradigm shift is being recorded that includes vibro-acoustics comfort in the set of critical design parameters. In the particular case of helicopters, this is mostly a consequence of a shift in the definition of the typical helicopter mission: in the past helicopters were mainly used in military context where flight mechanics, maneuverability and avionics are the key performance indicators; todays a trend is visible in the related industry that targets more and more civil applications, where the payload and environmental impact assume a much more significant role. In this respect, vibroacoustic comfort and more in general noise performance are becoming one of the key market differentiators: passenger comfort is included in the key performance indicators (ref. the US101 - Marine One case). In order to cope with this new and more stringent set of performance requirements, specific tools and techniques are required that allow better identifying the noise sources, the mechanics of transfer from source to target (pilot and/or passenger area) and defining an effective noise control strategy. In this scenario, the authors want to present a modus operandi to tackle these issues by several advanced experimental methodologies, since the requirement of a quieter helicopter needs a systematic study of its Noise Vibration and Harshness (NVH) behaviour. This chapter collects the results of several investigations carried out on two different helicopters: EUROCOPTER EC-135 and Agusta Westland AW-109. The proposed methodology faces these issues considering that the noise is a result of the contribution of source(s) reaching the receiver via various transmission paths. Therefore, in a noise control strategy , the designer should consider both the excitation phenomena (i.e. sources) as well as the transfer functions between the source(s) and receiver(s) (i.e. transmission paths). The sections of this chapter discuss both sources and transmission paths. In particular, Sections 2 addresses the deep analysis of transmission paths, taking into account the vibro-acoustic interaction that in cumbersome systems as helicopters is of pivotal importance; Sections 2 and 3 deal with noise and vibration sources,

while Section 5 presents a technique for gaining information about sources (operational forces) and transmission paths in operational conditions. Eventually, Section 6 presents an original approach based on sound synthesis allowing designers to listen and judge the sound quality impact of structural design modifications in a process of noise control and mitigation. It is interesting to note that although the presented methodologies concern particular helicopters, they have a general meaning, since they can be applied in a large variety of fields, as in aircraft fuselage, car or track interiors , etc. This work has to be intended as an analytical review of the authors' research (Mucchi & Vecchio, 2009; 2010; Pierro et al., 2009). Due to confidentiality reasons, several vibro-acoustical quantities reported in this chapter are presented without numerical values.

2. Noise control in coupled vibro-acoustical systems

Real-life enclosures, such as aircraft fuselage and car interiors, are very often characterized by a strong fluid-structure coupling (Desmet et al., 2003; Kronast & Hildebrandt, 2000). Therefore, the acoustical response in the cavity is related to the structural excitation and a relation exists between the acoustical loading and the structural responses as well (Everstine, 1997; 1981). Two methods are generally used to characterize the vibro-acoustical behaviour of such systems. In the first, the classical Experimental Modal Analysis (EMA), the modal parameters (natural frequencies, damping factors and mode shapes) are evaluated in laboratory, and consists in to put in vibration the system with a known excitation, out of its normal service environment. The common practice, indeed, is to make the peaks of the input force spectrum coincident with the valleys of the structural frequency response functions (FRFs). However, it is not so straightforward to get these tasks for vibro-acoustical systems because a modal analysis has a high number of theoretical and practical problems: due to the coupling, indeed, the system matrix is nonsymmetrical, yielding different right and left eigenvalues (but closely related). For this reason, care must be taken during the FRFs synthesis, but it has been proven that no matter involves in the modal model derivation itself (Wyckaert et al., 1996). The latter and more recent technique, is the Operational Modal Analysis (OMA), which does not require the knowledge of the operating forces on the system, but considers the assumption of white noise as input. Some investigations have been already made on vibro-acoustical operational modal analysis (Abdelghani et al., 1999; Hermans & Van der Auweraer, 1999), hereafter the modal decomposition in case of vibro-acoustical operational modal analysis is reviewed, in order to point out the influence on the modal parameter estimation of the references choice, i.e. acoustical or structural, used for the Cross power spectra calculation. The complete knowledge of the vibro-acoustical response of an helicopter cabin is a crucial tool for noise control purpose, and in the OMA context, it is strongly related to the reference choice rather than the input forces. For simplicity, only an acoustical input will be considered and the cross power between acoustical and structural responses will be derived and compared with structural cross power responses. The formulation in case of structural excitation can be derived in a similar way. The theoretical results have been verified through an experimental testing on the helicopter EUROCOPTER EC-135.

2.1 Vibro-acoustical systems

The dynamical properties of vibro-acoustical systems are presented hereafter. In particular the transfer function considering as excitation both the acoustical loading and the structural force and considering as response both the structural displacement and the acoustical pressure

is derived. It is well known that due to the fluid-structure interaction such systems are nonsymmetrical. Moreover, the FRF has a different form with respect to the decoupled systems. It is worth to stress that the non-symmetry is due to the choice of the variables **x**, **p**, **f** and $\dot{\mathbf{q}}$, being **x** the structural displacement, **p** the sound pressure, **f** the structural force and **q** the volume velocity. As stated above, due to the non-symmetry of the system, the right and the left eigenvectors, Ψ_r and Ψ_l, are different. Moreover the following relations can be proven (Ma & Hagiwara, 1991):

$$\left\{ \begin{array}{c} \Psi_{sl} \\ \Psi_{fl} \end{array} \right\}_{\lambda_h} = \left\{ \begin{array}{c} \Psi_{sr} \\ \frac{1}{\lambda_h^2}\Psi_{fr} \end{array} \right\}_{\lambda_h} \tag{1}$$

where subscript s is for the structural response location, f for the fluid (acoustical) response location, and λ_h are the roots of the system characteristic equation. In particular the following transfer functions obtained considering a structural force excitation f_j at location j, have been derived in (Wyckaert et al., 1996):

$$\frac{x_m}{f_j} = \sum_{h=1}^{n} \frac{(P_h)\,(\psi_{shm})\left(\psi_{shj}\right)}{(z-\lambda_h)} + \frac{(P_h)^*\,(\psi_{shm})^*\left(\psi_{shj}\right)^*}{\left(z-\lambda_h^*\right)} \tag{2}$$

$$\frac{p_p}{f_j} = \sum_{h=1}^{n} \frac{(P_h)\left(\psi_{fhp}\right)\left(\psi_{shj}\right)}{(z-\lambda_h)} + \frac{(P_h)^*\left(\psi_{fhp}\right)^*\left(\psi_{shj}\right)^*}{\left(z-\lambda_h^*\right)} \tag{3}$$

where x_m is the structural displacement at location m, p_p the acoustical pressure response inside the cavity at location p, P_h the modal scaling factors and n the number of modes in the frequency band of interest. Similar transfer functions can be obtained considering an acoustical excitation $\dot{q}$ at location k:

$$\frac{x_m}{\dot{q}_k} = \sum_{h=1}^{n} \frac{(P_h)\,(\psi_{shm})\left(\psi_{fhk}\right)}{\lambda_h^2\,(z-\lambda_h)} + \frac{(P_h)^*\,(\psi_{shm})^*\left(\psi_{fhk}\right)^*}{\lambda_h^2\left(z-\lambda_h^*\right)} \tag{4}$$

$$\frac{p_p}{\dot{q}_k} = \sum_{h=1}^{n} \frac{(P_h)\left(\psi_{fhp}\right)\left(\psi_{fhk}\right)}{\lambda_h^2\,(z-\lambda_h)} + \frac{(P_h)^*\left(\psi_{fhp}\right)^*\left(\psi_{fhk}\right)^*}{\lambda_h^2\left(z-\lambda_h^*\right)} \tag{5}$$

Considering $p = k$ and $j = m$ the vibroacoustical reciprocity, i.e. $(p_k/f_m) = -\left(\ddot{x}_m/\dot{q}_k\right)$, can be derived from (3) and (4). This modal description (Eqs.2-5) can be used for the parameter estimation (mode shapes, modal frequencies and damping factors) by means of standard algorithms.

Operational Modal Analysis (Peeters et al., 2007) is also called output-only modal analysis, and consists in a modal analysis without the knowledge and/or control of the input excitation. Assuming white noise as input, it enables to estimate the modal parameters from the cross power spectra (CPs) between the outputs and some responses chosen as references. In practice, the main difference with respect to the classical modal analysis is that the cross power spectra between the outputs are used to estimate the modal parameters, instead of the genuine FRFs (ratio between the system responses and the input forces). In vibro-acoustical systems the fluid-structure interaction yields both the acoustical and the structural outputs.

The power spectrum of the outputs, hence, can be obtained in three different forms, i.e. with acoustical outputs only, with structural output only and with both acoustical and structural outputs. Moreover, the input signal, supposed to be white noise, can be either structural or acoustical (or both of them simultaneously). In this section the results of the formulation of the operational modal analysis for vibro-acoustical systems are reported and discussed. For simplicity, only an acoustical input will be considered and the cross power between structural and the acoustical responses will be shown.

Let define the cross-correlation function $R_{mpk}(T)$ as the expected value $\mathbf{E}$ of the product of two stationary responses $x_m(t)$ and $p_p(t)$ due to the single $\dot{q}_k$ acoustical input at the kth degree of freedom (d.o.f.) evaluated at a time separation of T, i.e. $R_{mpk}(T) = \mathbf{E}\left[x_m(t+T)\, p_p(t)\right]$. Assuming white noise (i.e. $\mathbf{E}\left[\dot{q}_k(\tau)\,\dot{q}_k(\sigma)\right] = \alpha_k \delta(\tau - \sigma)$, with α_k a constant value related to the input and $\delta(t)$ the Dirac delta function) and performing some calculations, one obtains the cross power spectrum between *acoustical* f and *structural* s *responses*:

$$\left[\mathbf{G}_{fs}(i\omega)\right] = \sum_{h=1}^{n}\left[\frac{\{\Psi_s\}_h \left\{\mathbf{Q}_{fs}\right\}_h^T}{(i\omega - \lambda_h)} + \frac{\{\Psi_s\}_h^* \left\{\mathbf{Q}_{fs}\right\}_h^H}{\left(i\omega - \lambda_h^*\right)} + \frac{\left\{\mathbf{Q}_{fs}\right\}_h \left\{\Psi_f\right\}_h^T}{(-i\omega - \lambda_h)} + \frac{\left\{\mathbf{Q}_{fs}\right\}_h^* \left\{\Psi_f\right\}_h^H}{\left(-i\omega - \lambda_h^*\right)}\right] \tag{6}$$

with:

$$\left(Q_{fs}\right)_{ph} = \sum_{j=1}^{n} -\alpha_k \left[\frac{(P_h)\left(\psi_{fhk}\right)\left(P_j\right)\left(\psi_{fjp}\right)\left(\psi_{fjk}\right)}{\lambda_h^2\lambda_j^2\left(\lambda_h + \lambda_j\right)} + \frac{(P_h)\left(\psi_{fhk}\right)\left(P_j\right)^*\left(\psi_{fjp}\right)^*\left(\psi_{fjk}\right)^*}{\lambda_h^2\lambda_j^2\left(\lambda_h + \lambda_j^*\right)}\right] \tag{7}$$

$$\left(Q_{fs}\right)_{mh} = \sum_{j=1}^{n} -\alpha_k \left[\frac{\left(P_j\right)\left(\psi_{sjm}\right)\left(\psi_{fjk}\right)(P_h)\left(\psi_{fhk}\right)}{\lambda_h^2\lambda_j^2\left(\lambda_h + \lambda_j\right)} + \frac{\left(P_j\right)^*\left(\psi_{sjm}\right)^*\left(\psi_{fjk}\right)^*(P_h)\left(\psi_{fhk}\right)}{\lambda_h^2\lambda_j^2\left(\lambda_h + \lambda_j^*\right)}\right] \tag{8}$$

The unstable poles $-\lambda_h$ and λ_h^* derive from the negative time lags of the cross-correlation function $R_{mpk}(T)$. Consequently they can be deleted by means of the weighted correlogram approach determining the following half spectrum:

$$\left[\mathbf{G}_{fs}(i\omega)^{++}\right] = \sum_{h=1}^{n}\left[\frac{\{\Psi_s\}_h \left\{\mathbf{Q}_{fs}\right\}_h^T}{(i\omega - \lambda_h)} + \frac{\{\Psi_s\}_h^* \left\{\mathbf{Q}_{fs}\right\}_h^H}{\left(i\omega - \lambda_h^*\right)}\right] \tag{9}$$

The cross power spectrum between two *structural responses* s is:

$$\left[\mathbf{G}_{ss}(i\omega)\right] = \sum_{h=1}^{n}\left[\frac{\{\Psi_s\}_h \{\mathbf{Q}_{ss}\}_h^T}{(i\omega - \lambda_h)} + \frac{\{\Psi_s\}_h^* \{\mathbf{Q}_{ss}\}_h^H}{\left(i\omega - \lambda_h^*\right)} + \frac{\{\mathbf{Q}_{ss}\}_h \{\Psi_s\}_h^T}{(-i\omega - \lambda_h)} + \frac{\{\mathbf{Q}_{ss}\}_h^* \{\Psi_s\}_h^H}{\left(-i\omega - \lambda_h^*\right)}\right] \tag{10}$$

with:

$$\left(Q_{ss}\right)_{ph} = \sum_{j=1}^{n} -\alpha_k \left[\frac{(P_h)\left(\psi_{fhk}\right)\left(P_j\right)\left(\psi_{sjp}\right)\left(\psi_{fjk}\right)}{\lambda_h^2\lambda_j^2\left(\lambda_h + \lambda_j\right)} + \frac{(P_h)\left(\psi_{fhk}\right)\left(P_j\right)^*\left(\psi_{sjp}\right)^*\left(\psi_{fjk}\right)^*}{\lambda_h^2\lambda_j^2\left(\lambda_h + \lambda_j^*\right)}\right] \tag{11}$$

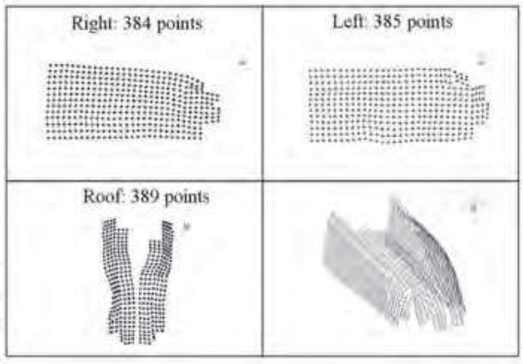

Fig. 1. Measured points of the cabin external surface.

$$(Q_{ss})_{mh} = \sum_{j=1}^{n} -\alpha_k \left[\frac{\left(P_j\right)\left(\psi_{sjm}\right)\left(\psi_{fjk}\right)(P_h)\left(\psi_{fhk}\right)}{\lambda_h^2\lambda_j^2\left(\lambda_h+\lambda_j\right)} + \frac{\left(P_j\right)^*\left(\psi_{sjm}\right)^*\left(\psi_{fjk}\right)^*(P_h)\left(\psi_{fhk}\right)}{\lambda_j^2\lambda_h^2\left(\lambda_j^*+\lambda_h\right)} \right] \tag{12}$$

By looking at Eqs. (6),(10) it is clear that the stable pole terms of the sum (i.e. the positive λ_h and λ_h^*) refer to the same mode shapes $\{\Psi_s\}_h$. The only differences between the two formulations are present in the output-only reference vectors $\{\mathbf{Q}\}_h$. Moreover, rewriting Eqs. (4) in a matrix form:

$$\left[\mathbf{H}_{fs}(i\omega)\right] = \sum_{h=1}^{n} \left(\frac{\{\Psi_s\}_h \left\{\mathbf{L}_f\right\}_h^T}{(i\omega-\lambda_h)} + \frac{\{\Psi_s\}_h^* \left\{\mathbf{L}_f\right\}_h^H}{(i\omega-\lambda_h^*)} \right) \tag{13}$$

it is evident that Eqs. (6),(10),(13), i.e. respectively the modal decompositions of OMA with an acoustical reference, OMA with a structural reference and vibro-acoustical EMA, depend on the same modal vector $\{\Psi_s\}_h$ and system poles λ_h. This means that in order to estimate the modal parameters (i.e. natural frequency and modal damping) it is possible to consider acoustical references instead of the structural ones as used in the common practice of OMA. This is useful for experimental campaigns aimed to a modal analysis of high scale vibro-acoustical structures for which it is common to take a microphone as reference inside the cavity, near the acoustical excitation. No additional reference sensors, hence, have to be located on the surface. In order to verify the practical effectiveness of the modal model obtained considering an acoustical reference (Eq.(6)), an operational modal analysis on a helicopter has been carried out, comparing the results with a classical EMA (Eq.(13)) where the input is the measured excitation (volume acceleration source).

2.2 Experimental application

A case study has been performed employing the data acquired from a test conducted on the helicopter EUROCOPTER EC-135. The EC-135 is a light twin-engine, multi-purpose helicopter with up to eight seats for pilot/s and passengers. Helicopters are typical examples of coupled vibro-acoustical systems related to a cavity environment. The experimental tasks about these systems mainly regard noise sources identification and modal parameter extraction. In this context, experimental and operational modal analyses are typically used to make the spaced peaks of the input force spectrum coincident with the valleys of the structural frequency response functions, for noise reduction purpose. These two analyses have been

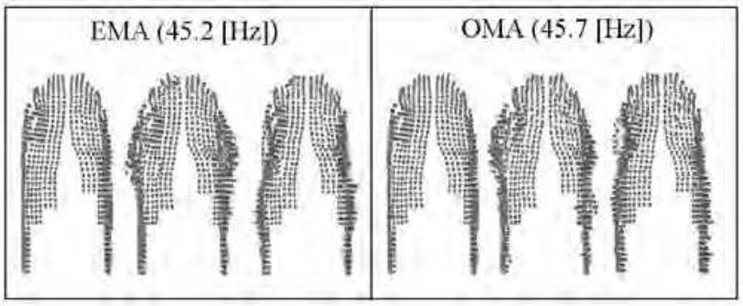

Fig. 2. First mode shape; bottom view of the helicopter cabin.

performed on the cabin external surface of the helicopter while the cavity was excited by means of an acoustical loading. The setup and the results will be shown in the following.

2.3 Test setup

For these applications, acoustical excitation is often preferred since it is usually more practicable than placing a shaker. Moreover, the acoustics of the cavity is excited in a direct way and the measurements are more efficient. In this testing campaign, indeed, a low frequency volume acceleration source (frequency range $20 - 400$ Hz) has been located inside the cabin near the pilot's seat, exciting the structure with a random signal. A microphone near the loudspeaker has been used as reference. The structural responses of 1158 points on the right, left and roof part of the cabin external surface (Figure 1) have been measured through a 4x4 PU sensors array, with a 10 cm spacing between the sensors both horizontally and vertically. The PU probes, integrate in a unique casing a hot-wire particle velocity sensor and a very small pressure transducer. They are, hence, specially conceived sensors for measuring acoustic intensity. The distance between the PU probes and the surface, indeed, can be so short that the very-near-field assumption is verified, i.e. the particle velocities simply represent the velocities of the cabin surface (in the normal direction) (De Bree et al., 2004). This is due to the particle velocity level, which is just slightly dependent on the distance to the object and not on the frequency. The very-near-field is a sound field very close to a source, where the particle velocity level is elevated compared to the sound pressure level and a phase shift between sound pressure and particle velocity is observed. The two conditions of the very near field are i) the measurement distance should be closer than the structural size of the object divided by 2π and ii) the wavelength of the sound should be larger than the structural size of the object. At last, the possibility of getting with just one measurement the needed data for both a modal analysis and an acoustic intensity calculation highlights the usefulness of these PU probes in this field, instead of classical methods such as accelerometers and scanning laser vibrometers. This point will be shown more in deep hereafter.

2.4 Test results

The results obtained by the two analyses, i.e. EMA and OMA, are shown in the following. In particular the aim is to experimentally verify the effectiveness of the parameter estimation obtained considering an acoustical reference in the OMA analysis, as theoretically predicted through the comparison between the formulation derived in Section 2.1 (Eq.(9)) and the vibro-acoustical EMA (Wyckaert et al., 1996) (Eq.(13)). Tab.1 lists the results in terms of natural frequency F_n for the modes lying in the $20 - 200$ Hz frequency range. In addition, the modal assurance criterion values (MAC) between the two analyses are given in Tab.1.

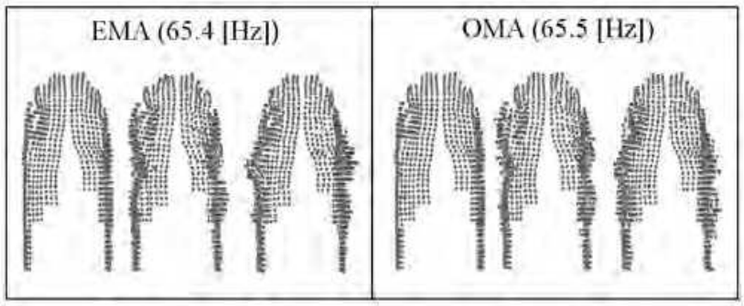

Fig. 3. Second mode shape; bottom view of the helicopter cabin.

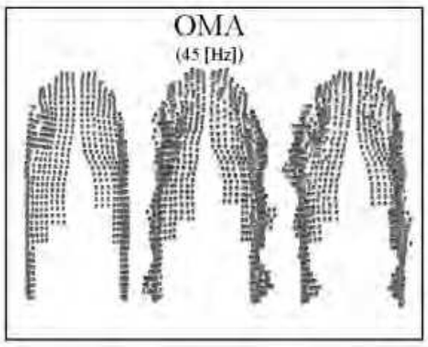

Fig. 4. OMA – first mode shape, full spectrum; bottom view of the helicopter cabin.

Mode	EMA	OMA	MAC	ΔF_n
	F_n [Hz]	F_n [Hz]	[%]	[%]
1	45.2	45.7	36.5	1.22
2	65.4	65.5	63.7	0.21
3	85.3	84	68.6	1.5
4	98.3	98.3	74.5	0.02
5	108.6	108.8	82.5	0.21
6	123.2	124.4	76.4	0.88
7	139.2	139.1	70.1	0.11
8	167.6	168.5	69.2	0.52
9	188.0	189.5	47.4	0.78

Table 1. Comparison of modal parameters from EMA and OMA.

The agreement between the two analyses for both the frequencies and the damping ratios is very good. In particular, a percentage difference between the frequencies, defined as $\Delta F_n = \left(\left|(F_n)_{EMA} - (F_n)_{OMA}\right| / (F_n)_{EMA}\right) * 100$, is always less than 2 %. The correlation values between EMA-OMA listed in Tab.1 are good, except for the first mode and the last one. For what regards this first mode, the reason could be the low excitation of the structure, in fact around that value the loudspeaker has its low frequency limit. On the other hands, the higher is the frequency the more it is difficult to get high correlation values, due to the higher number of local modes. This could be the reason of the low MAC value at the last frequency listed in Tab.1. The first 2 mode shapes obtained from the two analyses are visualized in the helicopter model (bottom view) in Figures 2 and 3. The comparison is a further confirm of the agreement

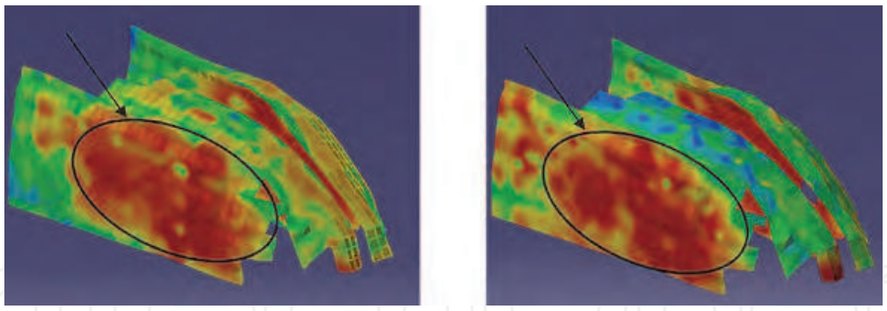

Fig. 5. 45.2 [Hz]: First mode shape on the left, intensity map on the right

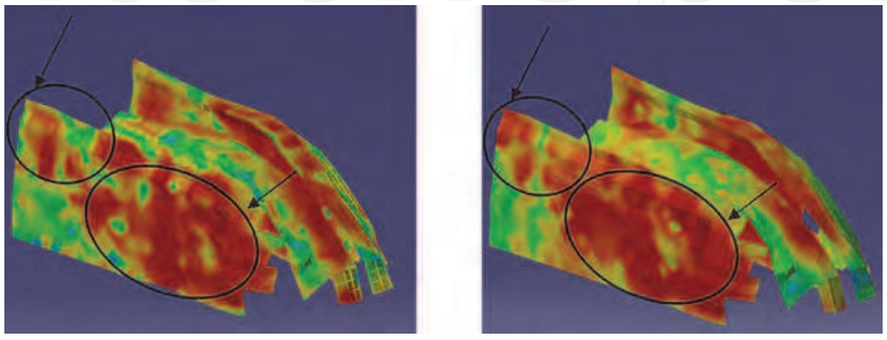

Fig. 6. 65.4 [Hz]: Second mode shape on the left, intensity map on the right

between the two analyses. In order to check the influence of the pre-processing of the CPs on the modal parameter estimation, an OMA analysis considering the CPs-full spectra, i.e. Eq.(6) as input, has been made. Figure 4 shows the first mode shape in such case. A comparison between Figure 4 (OMA full spectrum) and Figure 2 (EMA and OMA half spectrum) clearly highlights the bad numerical conditioning influence as a result of the unstable poles which are present in the full spectrum case. Figure 5 shows the comparison for the first mode (i.e. 45.2 Hz). The red zones indicate the maximum displacements for the mode shapes and the hot spots calculated with the intensity maps. Figure 5 and Figure 6 confirm the good choice of the modes. It is evident, indeed, the correspondence between the zones with high intensity values and the zones with the highest modal displacements (circled areas).

2.5 Further discussions on vibro-acoustical coupling

It is of crucial importance, for the noise control in the cabin interior, the vibro-acoustical coupling assessment between the cabin internal surface and the enclosure.
By means of different EMA on the helicopter, it has been shown that the cabin external surface is coupled to the interior as well as the internal part. Moreover, the mathematical formulation of the CPs modal decomposition in case of vibro-acoustical operational modal analysis has been presented in the previous subsections, clarifying the influence on the modal parameter estimation of the references choice, i.e. acoustical or structural, used for the CPs calculation.
The relevance of such analyses is pointed out through the results of four different experimental analyses on the helicopter EUROCOPTER EC-135, i.e. an acoustical modal analysis (AMA) of the cabin enclosure, an EMA of the cabin internal surface, an EMA and an OMA of the cabin external surface, the latter considering a microphone inside the cabin as reference for the CPs calculation, as explained before.

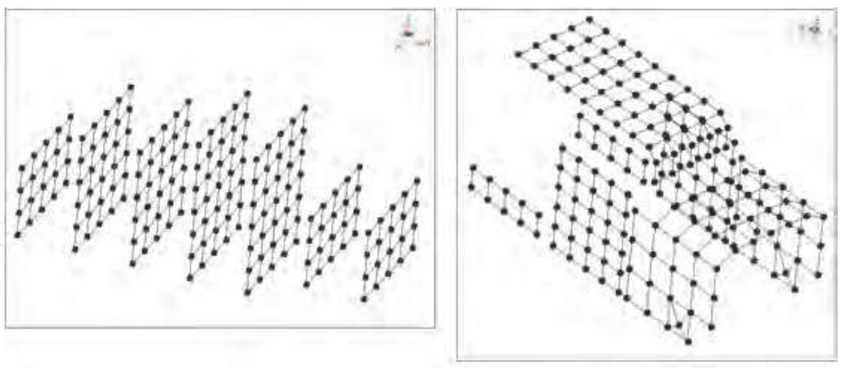

Fig. 7. Measured points in the helicopter cavity (left) by means of microphones and on the cabin internal surface (right) by means of accelerometers.

Mode	AMA-internal part		EMA-internal part		EMA-external part		OMA-external part	
	F_n [Hz]	ζ%	F_n [Hz]	ζ%	F_n [Hz]	ζ%	F_n [Hz]	ζ%
1	46.5	2.8	46.3	2.9	45.2	1.6	45.7	2.0
2	65.1	2.1	66.5	1.9	65.4	2	65.5	1.0
3	86.1	2.9	86.4	1.9	85.3	1.6	84	0.6
4	98.1	0.4	97.5	1.2	98.3	1.4	98.3	0.9
5	109.7	1.5	110.2	1.2	108.6	1.3	108.8	1.2
6	124.4	2.6	124.3	1.1	123.3	1.3	124.4	1.6
7	139.4	2.5	136.4	1.1	139.2	1.5	139.1	1.5
8	160.8	1.1	168.9	1.4	167.6	1.1	168.5	1.1
9	175.5	6.1	188.4	0.7	188	0.6	189.5	0.8
10	189	2.7	-	-	-	-	-	-

Table 2. Natural frequencies (F_n) and modal damping (ζ) for the four analyses performed on the helicopter cabin.

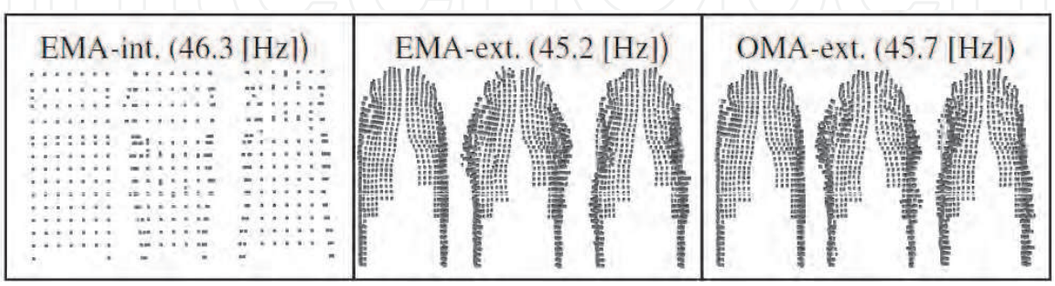

Fig. 8. First mode shape; bottom view of the helicopter cabin, internal (left) and external surface (second and third on the right).

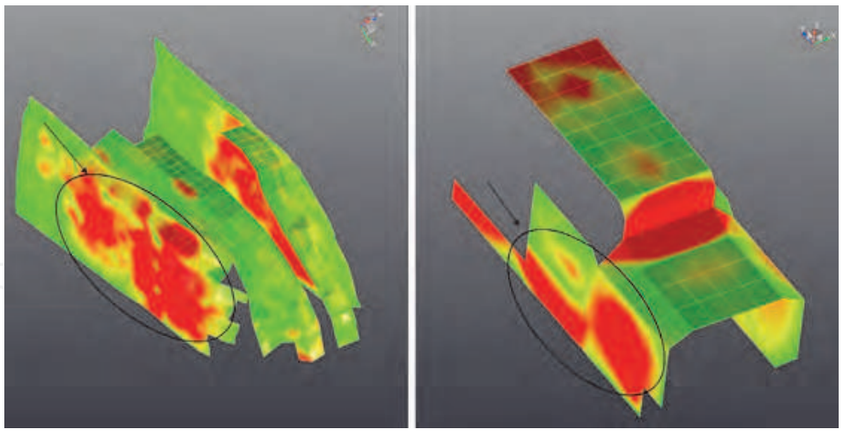

Fig. 9. First mode shape coloured map of the cabin external surface (left) (45.2 Hz) and the cabin internal surface (right) (46.3 Hz)

In the helicopter internal part two measurements were carried out aiming at performing an acoustical modal analysis of the cabin enclosure and a classical modal analysis of the cabin internal surface. Figure 7 (left) shows the 190 points measured by means of condenser microphones (1/2" prepolarized) inside the cavity and the acceleration of the cabin internal surface measured by means of accelerometers (1-10kHz of frequency range) on 195 points, in the left, right and roof part. A horizontal bar, holding five microphones spaced by 25 cm, was used to measure the acoustical responses of the enclosure. Seven measurement planes were considered, spaced by 50 cm, while the vertical spacing between the lines was 20 cm. The accelerometers were mounted on the inside walls of the cabin, measuring only the surface normal acceleration (Figure 7, right). The measurements on the interior of the cabin lead to collect two set of FRFs: pure-acoustical FRFs $[\mathrm{Pa}/(\mathrm{m}^3/\mathrm{s}^2)]$ for the cavity and acoustical-structural FRFs for the cabin internal surface $[(\mathrm{m}/\mathrm{s}^2)/(\mathrm{m}^3/\mathrm{s}^2)]$. In Tab.2 the results for the modes lying in the 20-200 Hz frequency range are listed for each analysis, in terms of natural frequency F_n and modal damping ζ. A few remarks can be done about the modal properties (F_n and ζ) obtained from the analyses. At first, the cabin external surface is evidently acoustically coupled to the enclosure. In fact, as the first and the third columns of Tab.2 clearly indicate, the walls of the helicopter cabin (structural parts) vibrate at the same natural frequencies as the cabin internal cavity (fluid part). A further validation can be obtained by a visual inspection of the maps shown in Figure 8 and Figure 9. This implies important consequences concerning the identification of the entire coupled behaviour.
Secondly, the modal properties obtained from the OMA analysis performed by means of CPs, i.e. the cross power spectra between the external walls response and the internal acoustical reference, clearly confirm that an acoustical reference is enough efficient. However, once the coupling between the cabin external surface and the cavity has been assessed, and the most appropriate excitation method has been chosen, it is important to point out that a structural response could be taken as reference in any case; so, in this scenario a structural point fully coupled to the enclosure can be provided as reference, without any risk to loss coupled modes. Obviously, this condition is not straightforward to be a-priori satisfied, and therefore it is more clear now the convenience related to an acoustical reference, since the coupled modes will be surely identified.

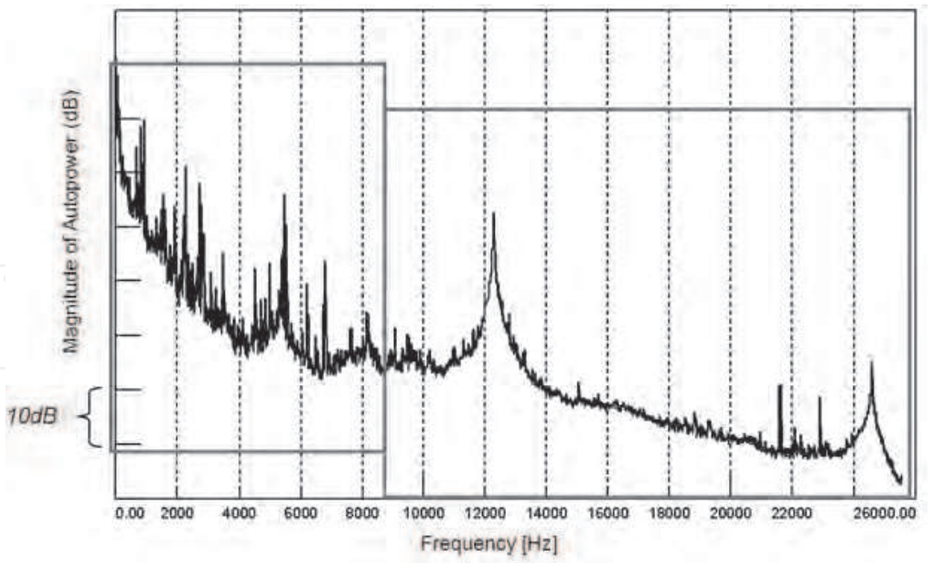

Fig. 10. Autopower of the acoustical pressure measured by the pressure probe of a PU probe in the internal surface of the helicopter cabin (roof) in the steady-state operational condition.

3. Noise control with vibro-acoustical signature analysis

Since the main vibration excitations on the helicopter units are mechanical and aerodynamical (Gelman et al., 2000), the generated noise in operational conditions can be distinguished in aerodynamic-borne and mechanic-borne noise; aerodynamical noise is not considered here, but an exhaustive analysis can be found in (Conlisk, 2001) both from an experimental as well as a numerical viewpoint. Mechanical noise is due to the contribution of the gearbox and to the contribution of the jet engines. In the case of helicopter gearboxes, there is a very wide range of shaft frequencies, and the associated meshing frequencies and bearing frequencies cover the low-medium audio frequency range. Since the power engine of a helicopter is characterized by high rotational speed (about 30000 RPM) the generated noise due to the turbine and compressor blades mainly lies in the high frequency range (10-20kHz), but the harmonics of the turbine and compressor shaft still remain in the low-medium frequency range where the human ear is strongly sensitive. Noise control in helicopter first of all requires a systematic study of its NVH (Noise Vibration and Harshness) behaviour, with special attention to helicopter operational conditions. Furthermore, sound quality is of great importance in achieving sound which is agreeable to the human ear, in fact noise annoyance not only depends on sound exposure levels. For these reasons the authors have performed a wide experimental vibro-acoustic campaign in a helicopter interior cabin. Substantially, the study has two main goals: the first goal is to give a systematic methodology for defining the NVH behaviour of an helicopter in steady-state and run up operational conditions by using efficient and fast experimental techniques; the second goal is to evaluate the importance of the noise contribution produced by the jet engines with respect to the gearbox.

3.1 Case history and experimental setup

The signature analyses presented in this work have been performed employing the data acquired from experimental tests conducted on the helicopter EUROCOPTER EC-135. The data have been acquired in operational conditions in which the helicopter was clamped on

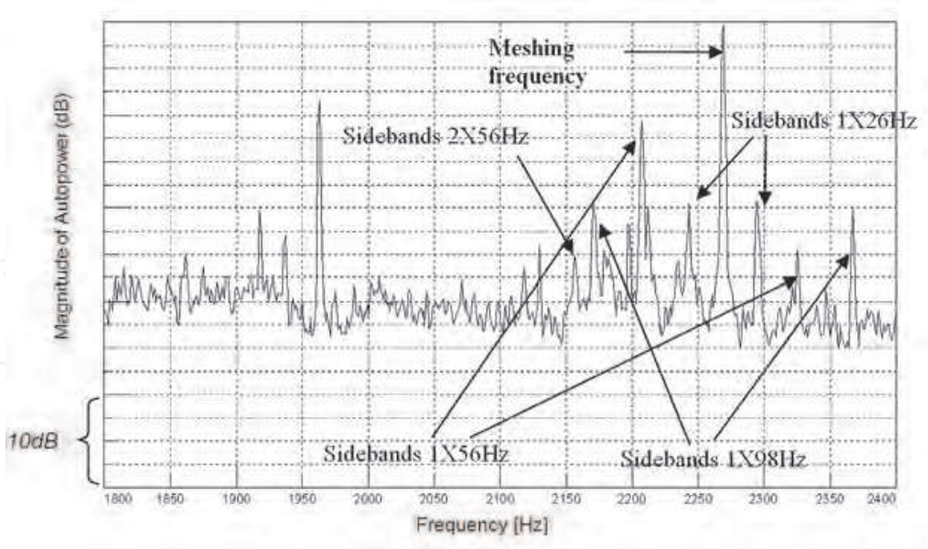

Fig. 11. Autopower of acoustical pressure. Zoom of Figure 10 around a meshing frequency (from 1800Hz to 2400Hz). Meshing frequency and relative sidebands spaced at 26Hz 56Hz, and 98Hz.

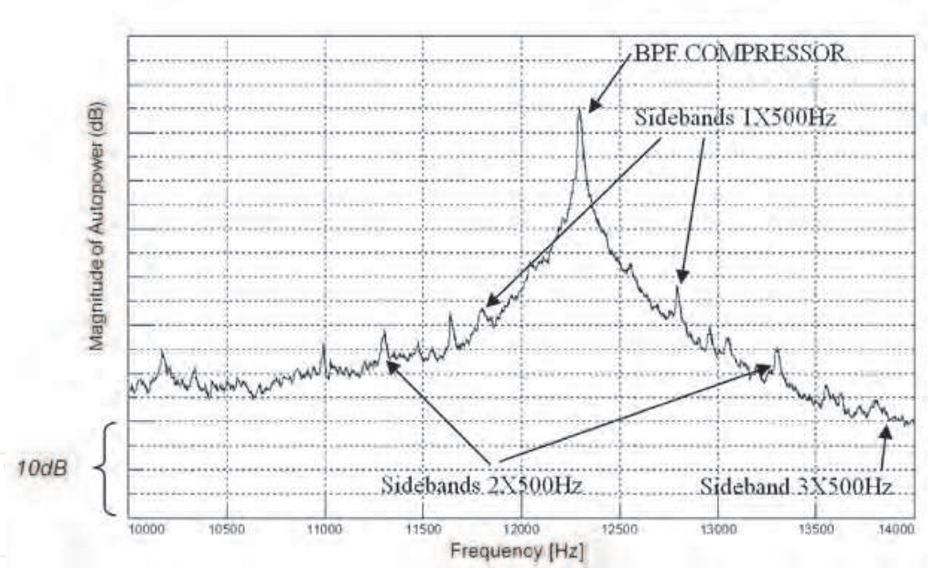

Fig. 12. Autopower of acoustical pressure. Zoom of Figure 10 around the Blade Passing Frequency of the first stage of the compressor. BPF and relative sidebands spaced of 500Hz (corresponding to the frequency of rotation of the compressor shaft).

the ground while the engines were limited to 60% of the maximum power and the two rotors giving power to the main blades and to the tail blades were activated. This operational condition can be considered representative of a possible helicopter operational condition since we are interested in the mechanical-borne noise only and not in the aerodynamical noise. Such tests were performed in steady-state operational conditions (constant main blade speed) and for a run up.

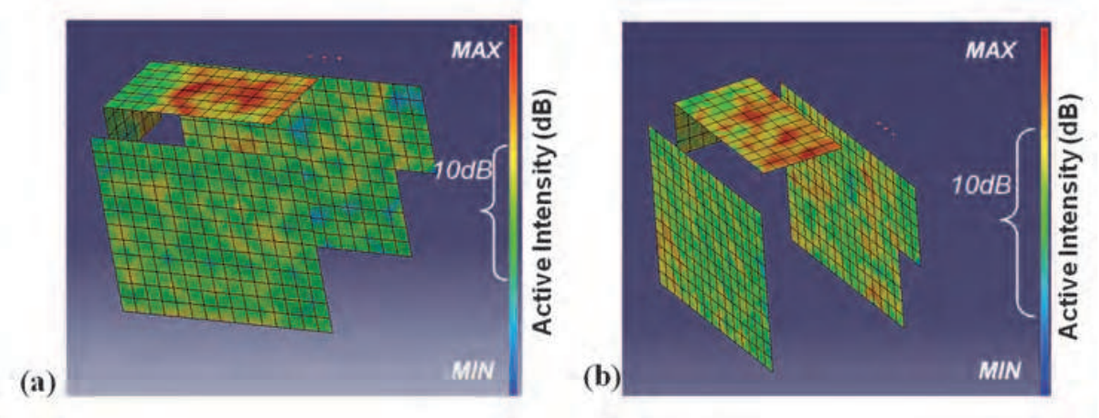

Fig. 13. Active intensity maps on the cabin internal surface at the first (a) and second (b) harmonic of BPF of the first stage of the compressor in dB scale.

The acoustical experimental tests concern measurements in the internal surface (see Figure 7, right) of the helicopter cabin by using the 4×4 PU sensor array, described in Section 2.3. The PU sensor array was positioned close to the internal walls so the very near field assumption is verified (De Bree et al., 2004). The active acoustic intensity is then evaluated as the real part of the crosspower between pressure and particle velocity. The information containing the location of the measured points (see Figure 7, right) and the active acoustic intensity data allows a 3D representation of the intensity map as shown hereafter. Simultaneously with the signals coming from the PU probes, the horizontal bar holding eight condenser microphones (described in Section 2.5) was used to acquire the noise in proximity of the right and left side of the helicopter internal cabin. Some acceleration measurements were taken too in order to obtain the operational deflection shapes (ODS) of some panels of the cabin; in particular, forty piezoelectric accelerometers (frequency range 1 to 10000 Hz) were positioned inside the cabin on the roof (30 accelerometers) and on the door panels (5 accelerometers each side), measuring only along the perpendicular direction of the panels. The ODS analysis has been performed in order to assess the results obtained by the PU probes.

3.2 Signature analysis in steady-state operational conditions

Hereafter the discussion concerning the steady-state operational conditions is presented. Figure 10 shows a typical example of the autopower of the pressure probe of a PU on the roof; two different zones can be easily distinguished: the low frequency range (0 till about 8kHz) is dominated by the rotational frequencies, meshing frequencies and relative harmonics concerning the gearbox (main transmission) whilst in the high frequency range (8kHz-25kHz) the pivotal role is played by the jet engines, and the compressor in particular (due to confidentiality reasons, the curve amplitude is represented without numerical values). In fact, the power transmission of a helicopter is divided into two main parts: one concerning gearing (gearbox) and one concerning the jet engines (composed of compressors, combustion chambers and turbines). Due to the different rotational speed of the turbines and compressor with respect to the shafts in the gearbox, the relative harmonics lie in different frequency ranges. It is a matter of fact that the turbines and compressor rotate at about 30000 RPM while the shaft of the main blades rotates 100 times slower (at about 350 RPM), In particular, for the gearbox, the meshing frequencies related to the input gear, the bevel/spur gears in some intermediate shafts, the collector gear in the pinion shaft and the spur/bevel gear

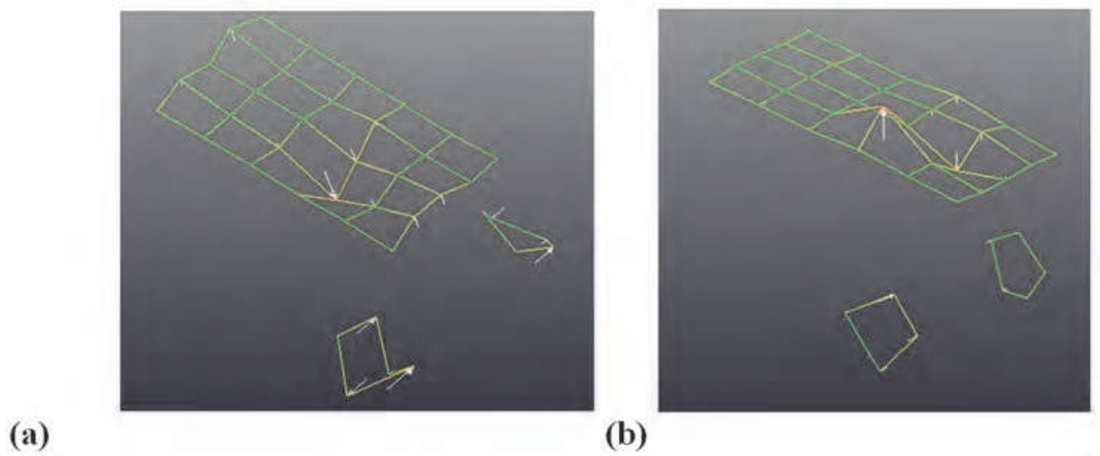

Fig. 14. Operational deflection shapes at the first (a) and second (b) harmonic of BPF of the first stage of the compressor obtained by acceleration measurements on the internal surface of the helicopter cabin.

in the hydraulic pump shaft lie in the low frequency range (till 3000Hz) and their main harmonics excite the medium frequency range (till about 8kHz). On the other hand, the harmonics of the blade pass frequencies and vane pass frequencies of the compressor and turbine lie in the high frequency range (10kHz-20kHz) due to the high rotational speed of the shafts and the high number of blades. Figure 11 shows a zoom of Figure 10 in the low frequency range; three sideband families spaced at a frequency corresponding to the rotational speed of the three shafts involved in such a meshing appear around each meshing frequency. Similar characteristics exhibit the harmonics related to the blade pass tones of the compressor stages; in particular Figure 12, representing a zoom of Figure 10 around 12kHz, shows the peak related to the first stage of the compressor: it is very common in helicopter jet engines for the first stage of the compressor to have the BPF component of high amplitude. Furthermore, usually it is also higher than the amplitude of the harmonics related to the turbine BPF, as confirmed in (Gelman et al., 2000). Several sidebands appear around the blade pass frequency (BPF) as occurs around the meshing frequencies; the sidebands around a certain main frequency specify the rotational frequency of the relative shaft and in this case such sidebands are spaced at 500Hz corresponding to the compressor shaft rotational speed (30000 RPM). The peak at about 25 kHz depicted in Figure 10, represents the second harmonic of the BPF of the first compressor stage.

Figure 13 shows the intensity map obtained by means of the PU probe measurements on the internal cabin in operational conditions at the frequency corresponding to the first and second harmonic of the BPF of the first stage of the compressor (the dB values are omitted for confidential reasons). The amplitude is clearly high in correspondence to the roof surface (red color) highlighting the high level of excitation coming from the jet engine location. An example of operational deflection shape (ODS) analysis performed by means of the accelerometer measurements on the cabin roof and lateral doors is represented in Figure 14; in particular the figure highlights the same behaviour as the intensity map at the frequency corresponding to the first and second harmonic of the BPF of the compressor. In fact the ODSs show large deflections in the roof panel at such frequencies. So, the intensity map and the ODS analysis can be considered very useful tools for source identification and relative quantification.

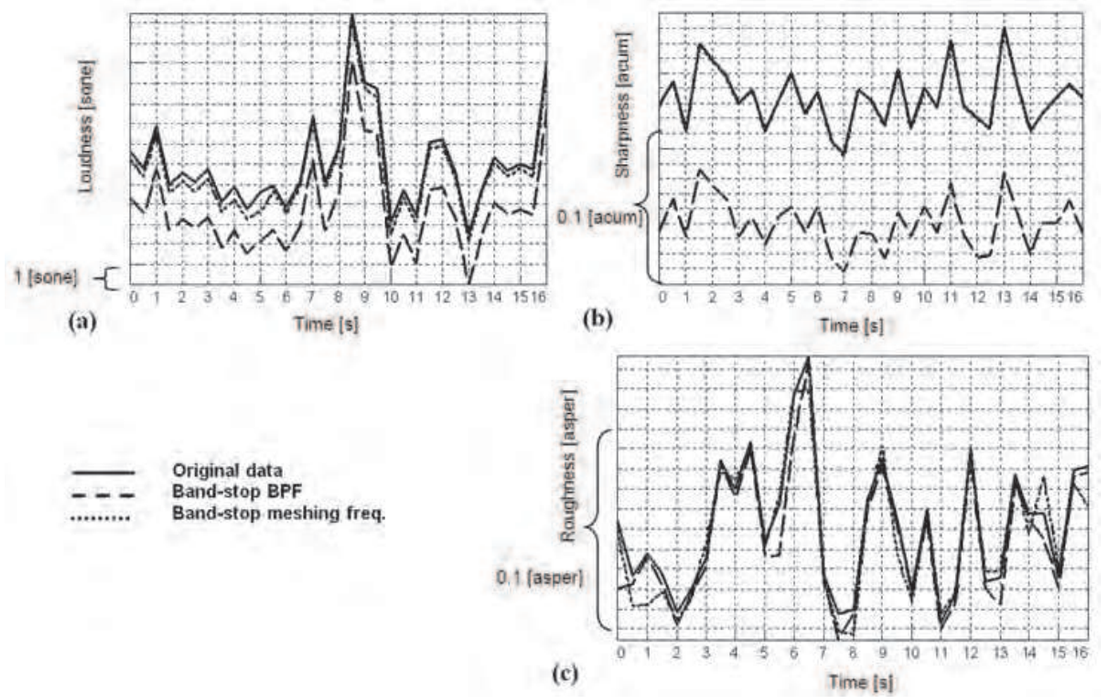

Fig. 15. (a) Loudness Stevens 6, (b) Sharpness and (c) Roughness of the acoustic pressure in the interior of the helicopter cabin (roof) in linear scale: original row data, data filtered with a band-stop filter around the BPF of the compressor of Figure 12 and data filtered with a band-stop filter around the meshing frequency of Figure 11.

Finally, by using the acoustic pressure data coming from the eight microphones, some metrics parameters (Loudness, Roughness and Sharpness) (Zwicker, 1999) are calculated. It is well known that *Loudness* is a perceptual measure of the effect of the energy content of a sound on the human ear, *Sharpness* is a measure of the high frequency content of a sound - it allows classification of sounds as shrill/sharp or dull - while *Roughness* (or harshness) is a quantity associated with amplitude modulations of tones. The curves in Figure 15 show such metrics parameters regarding the row data (solid line) and the band-stop filtered data (dotted lines); in particular the filtered data are obtained neglecting the contribution of the first harmonic of the BPF of the compressor and the first harmonic of a meshing frequency of the gearbox. The curves are obtained filtering the data by a band-stop digital filter around the meshing and blade pass frequency in Figure 11 and Figure 12, respectively. Comparing the filtered data with respect to the row data a notable difference occurs, in particular it can be seen that the Loudness and the Sharpness of the signal without the compressor harmonic is always the lowest, confirming that jet engine noise plays an important role in global perceived noise. The curves related to the Sharpness of the row data and the band-stop filtered data around the meshing frequency are overlapped: this behaviour was expected since such a meshing frequency lies in the low frequency range. The Roughness is obviously the same in the three cases because the degree of modulation is the same: the band-stop filter involves only the main frequency and not the sidebands (i.e. the modulation effect). In such a metric parameter comparison, the first meshing harmonic of the input gear in the gearbox and the BPF of the first compressor stage have been involved because they are representative of important gearbox and jet engine noise phenomena.

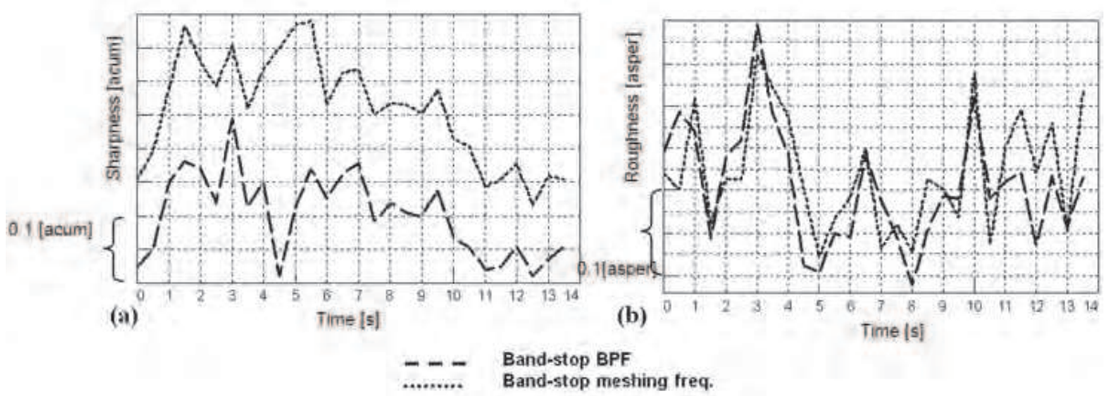

Fig. 16. Sharpness (a) and Roughness (b) of the acoustic pressure in the interior of the helicopter cabin (roof) during the run up (linear scale): data filtered with an order-stop filter around the BPF of the compressor of Figure 13 and data filtered with a order-stop filter around the meshing frequency of Figure 12.

3.3 Signature analysis during a run-up

The run up test was performed gradually increasing the main blade speed, reaching 60% of the maximum power after 14 seconds with the aim at performing a sound metric comparison as performed in the steady-state condition by filtering the contribution of the compressor BPF and the contribution of the meshing frequency of the input shaft in the gearbox, an accurate order tracking technique is hereto essential.

The idea is to apply an order filter to the run up spectrum for deleting the contribution of the meshing frequency of the input shaft and the contribution of the BPF of the compressor as done in the steady-state condition. It has to be underlined that the rotational speed of the input gear in the gearbox and the rotational speed of the compressor are different and not proportional, due to the variable transmission ratio in between. Therefore, two different order tracking analyses have to be performed, one tracking the signal with the RPM curve of the input shaft and one tracking the signal with the RPM curve of the compressor shaft. Since a tacho reference was not available, a tacholess RPM extraction method has been applied (Mucchi & Vecchio, 2010) .Then, a few sound metrics parameters (Roughness and Sharpness) are calculated from the filtered data and depicted in Figure 16; the Sharpness without the contribution of the compressor order shows lower values with respect to the curve without the contribution of the gear meshing, meaning that the compressor is responsible for the shrill sound produced by the helicopter (see Figure 16(a)). Concerning the Roughness comparison, it can be noted that, as in the steady-state condition, the values are similar (Figure 16(b)) because the order filter used does not reduce modulation effects in the signal.

4. Ultrasonic and acoustical intensity measurements for fast leakage spot detection

Leakage points are possible noise sources or locations through which noise can propagate, they are due to non-homogeneity, fractures or cavities in the material, defects during assembly (e.g. improper alignment of the seals along the cabin doors or incorrect coupling between cabin surfaces due to split rivets), etc. The detection of leakage points on the cabin surface is of high interest for NVH designers and can be a useful tool for quality and noise control. In fact, such points can cause high noise levels in the cabin since they can excite the acoustical

Fig. 17. Leakage points (in red) on the helicopter cabin found by means of the ultrasound technique (cabin right panels)

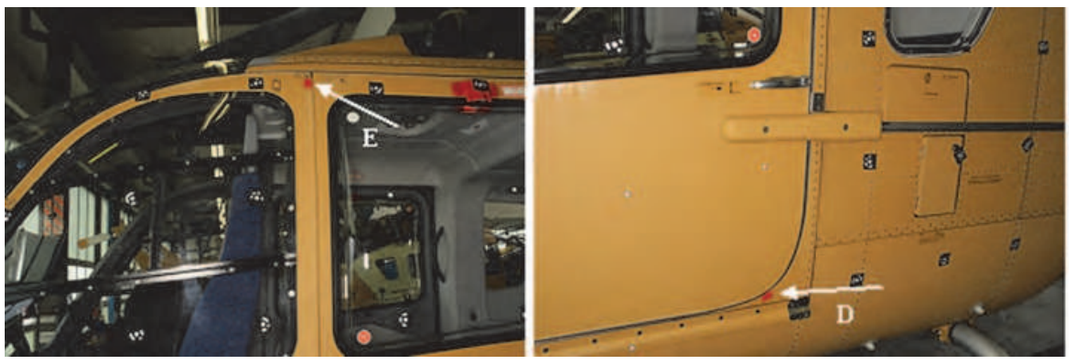

Fig. 18. Leakage points (in red) on the helicopter cabin found by means of the ultrasound technique (cabin left panels).

resonances of the enclosure and determine human discomfort during flight. Commonly, leakage point detection is performed by using an ultrasonic transmitter/receiver; in this section, the authors present how to find leakage points by means of the acoustical intensity analysis as an useful and precise tool for their localization and quantification.

The ultrasonic technique makes use of ultrasound transmitter/receiver and the acoustical intensity analysis is performed by using PU probes. This second technique is performed in operational conditions and in controlled conditions (i.e. where the excitation is measured and applied by using a volume acceleration source). Both techniques have their advantages and disadvantages that will be explained later on.

Ultrasonic sensors (Wallace, 1972) utilize transducers, which transform an electrical signal into an ultrasonic wave and vice versa. Ultrasound covers a frequency range from 20kHz to about 1 GHz, however for technical applications the range 20kHz to 10MHz is the most important one. Ultrasound enables instruments to be non invasive and also non intrusive because the acoustic wave can penetrate walls. Furthermore, high frequency sounds are more directional than lower frequency ones: this makes it easier to pinpoint the source even in the presence of other background noise. Obviously, the propagation of acoustic waves through multi-layered structures depends on the acoustics impedance mismatch at each of the boundaries the ultrasound has to pass, furthermore it depends on the attenuation of the ultrasound in the different materials and finally in some cases on the relationship between the wall thickness and the wavelength of the ultrasound waves. In particular, firstly an ultrasonic transmitter (SDT 8MS) producing an omni-directional tonal noise at the frequency of about

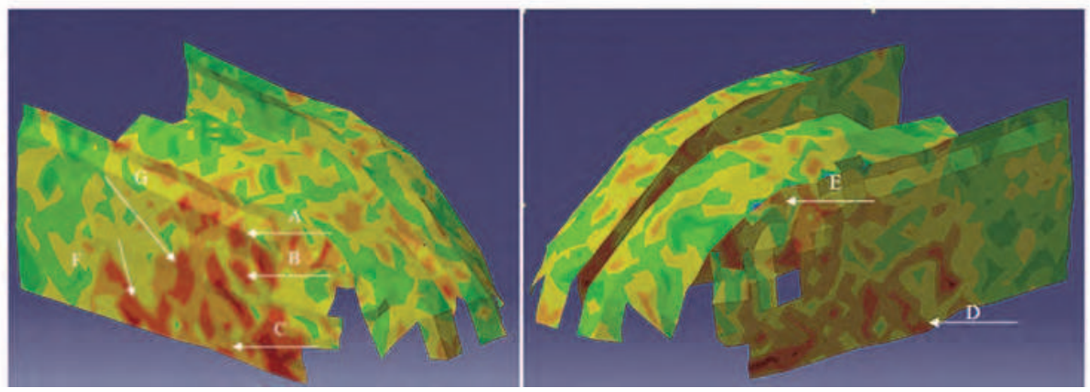

Fig. 19. Intensity map in dB of the cabin external surface at the meshing frequency of the input gear in the gearbox.

40kHz has been used inside the helicopter cabin while the ultrasonic receiver (SDT 170) was on the external surface of the cabin scanning the entire external cabin surface. Thus, the location of the leakage points can be evaluated by this first simple measurement, in fact when the receiver detects a point through which the level of ultrasonic noise exceed a threshold level, an audio sound signal occurs highlighting a leakage point. This measurement deals with the transmissibility of the tested surface to the ultrasonic waves. Obviously, the surface transmissibility is increased in correspondence of fracture or in-homogeneity on the material, malfunctioning of the seals, etc. It is important to underline that in helicopter operational conditions, the noise comes from the exterior to the interior of the helicopter cabin, on the contrary during this first measurement, as well as on the further measurements described hereafter, the noise comes from the interior (by means of the ultrasonic transmitter) and the detection is performed on the exterior. This can be considered acceptable under the assumption that the helicopter cabin satisfying the reciprocity principle, as demonstrated in (Pintelon & Schoukens, 2001). Furthermore, in order to localize the leakage points with more spatial precision, a second ultrasonic measurement is carried out exciting on the internal cabin side in correspondence of the above-detected leakage points and measuring the value of the wave crossing the cabin panel (from the interior to the exterior) by means of the same ultrasonic receiver. In this second test, an ultrasonic transmitter (SDT 200mW) producing a one-directional tonal noise at the frequency of about 40kHz has been used as excitation inside the cabin giving more accuracy in the measurement.
Figure 17 and Figure 18 show the leakage points (red dots in the figures) found by means of the above-described ultrasound technique. These points represent locations where the ultrasound wave can propagate from the interior to the exterior, in particular they are located on the boundary of the doors where the seal between the door and the cabin is not so efficient from an insulation viewpoint. The knowledge of the location of these defects is of primary importance for the designer that has to find solutions in order to improve the cabin insulation. In fact, the test is carried out exciting the interior of the cabin ad measuring in the exterior, but as stated before, due to reciprocity, the same results can be obtained exciting the exterior and measuring the ultrasound wave on the interior of the cabin. This means that such a test gives information about the locations from which the acoustic radiation can propagate on the cabin impoverishing the acoustic comfort of the passengers and pilots.

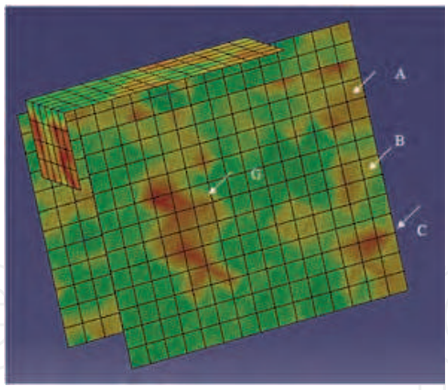

Fig. 20. Intensity map in dB of the cabin internal surface at the meshing frequency of the input gear in the gearbox

Similar results can be obtained from the intensity maps of the external surface (Figure 19, the dB values are omitted for confidential reasons). As described in Section 1.3 such a test is carried out exciting the cabin from the interior side with a flat broadband noise (white noise), then the active acoustic intensity is evaluated as the real part of the crosspower between pressure and particle velocity, being the measurements carried out by PU probes. In Section 2.4 the same measurements were used for EMA purpose obtaining the mode shapes at the natural frequencies, here the sound intensity maps are evaluate at every frequency in the measured frequency range. Such maps depicted at the natural frequency of the cabin are obviously similar to the mode shapes of the cabin external surface, due to the contribution of the particle velocity acquiring in the very near field and being representative of the structural vibration of the panels. On the other hand, the maps depicted at frequency far from the natural frequencies and for example corresponding to the tonal excitations of the gearbox (e.g. meshing frequency of the collector gear in the pinion shaft, or meshing frequency related to the input gear) highlight high intensity values in the same locations as the pictures of Figure 17 and Figure 18 shown (compare same characters on the figures). In fact the active intensity represents the energy flow that a surface radiates and therefore is very sensible to leakage point localization.
Figure 20 shows an example of intensity map on the internal surface obtained in operational conditions and depicted at the frequency corresponding to the meshing frequency of the input shaft in the gearbox. The map is able to identify the same leakage points found by the intensity map on the external surface and by the ultrasound technique (consider the corresponding characters in Figures 17, 18, 19). It is interesting to note that both the ultrasound techniques and the intensity measurements are effective tools for the identification of leakage points. The first technique is simpler to apply, the cost of the instrumentation needed is cheaper than the second techniques, but the intensity maps gives more information than ultrasonic techniques, in fact since they represent the active sound intensity they are effective for panel efficiency evaluation too (Wallace, 1972). Moreover the intensity maps can be calculated on the entire measured frequency range, allowing calculation of the energy flow dissipated by the leakage points as a function of frequency.

5. Vibro-acoustic transfer path analysis

Noise levels recorded in helicopters' cabin are severely affected by the strength and vicinity of noise sources. The jet engines, the gearbox and the rotors can be considered as

separated sources - whose spectral content is strongly tonal and RPM dependant - exciting simultaneously the cabin's acoustic cavity. Under the hypothesis of linear behaviour, the total sound pressure level measurable in the cabin can be considered as the summation of a number of partial pressure contributions, each generated by one source acting separately. The mechanism responsible for transferring the mechanical energy from each sources to the target location can be either structure borne - via the mechanical joints connecting the gearbox to the helicopter's frame - or airborne - via the sound propagation in the air. Some transfer paths may cause interference at certain frequencies such that the observer does not notice anything significant- until he moves position. Transfer Path Analysis (TPA) represents a techniques used to assess the structure and air-borne energy paths among excitation source(s) and receiver location(s) in a process of noise control. TPA has been largely applied in the automotive industry that allows identifying the main transmission paths and their relative contribution to the total sound pressure level at target location. From a theoretical standpoint there is not reason why TPA should be limited to cars. An helicopter is a more complex system then a car, but this actually implies that there may be more noise sources, hence more transfer paths. An experimental TPA approach is hereby applied for the first time to the helicopter Agusta A109 (Vecchio et al., 2006), to assess noise source contribution to the cabin noise and to simulate a number of realistic noise reduction scenarios. Usually vibro-acoustic TPA involves measurements of accelerations in operational conditions and of vibration and/or vibro-acoustic transfer functions (TFs). The transfer functions can be measured using the most practical approaches – either using hammer or shaker or volume acceleration source excitation techniques. Briefly, the vibro-acoustic TPA is an analysis fully described by means of two sets of equations 14-15:

$$\begin{Bmatrix} F_1 \\ \vdots \\ \vdots \\ F_n \end{Bmatrix} = \begin{bmatrix} \frac{\ddot{X}_1}{F_1} & \frac{\ddot{X}_1}{F_2} & \cdots & \frac{\ddot{X}_1}{F_n} \\ \vdots & & & \\ \frac{\ddot{X}_m}{F_1} & & & \end{bmatrix}^{-1} \begin{Bmatrix} \ddot{X}_1 \\ \vdots \\ \vdots \\ \ddot{X}_m \end{Bmatrix} \tag{14}$$

$$\begin{Bmatrix} p_1 \\ \vdots \\ \vdots \\ p_q \end{Bmatrix} = \begin{bmatrix} \frac{p_1}{F_1} & \frac{p_1}{F_2} & \cdots & \frac{p_1}{F_n} \\ \vdots & & & \\ \frac{p_q}{F_1} & & & \end{bmatrix}^{-1} \begin{Bmatrix} F_1 \\ \vdots \\ \vdots \\ F_n \end{Bmatrix} \tag{15}$$

where $\{\ddot{X}_1 ... \ddot{X}_m\}^t$, $\{F_1 ... F_n\}^t$, and $\{p_1 ... p_q\}^t$ are the acceleration, the operating force and acoustic response vectors, respectively. Equation 14 brings into play the relation between the operating forces transmitted along the paths and the structural accelerations caused by these forces, while the second set of equations relates the acoustic responses, e.g. the noise inside a cabin, and the operating forces. Hence, it is pretty clear that by exploiting the information that the first set of equations carries it is possible to compute the acoustic responses from the second one. Indeed, it is much easier to measure the accelerations of a structure rather than the forces; these accelerations can then be employed in order to compute the operational forces which substituted in the second set of equations will lead to the final result. On the left hand side of equation 14, there are the operating forces. As it can be seen, it is necessary to invert the matrix linking the accelerations and the forces. This constitutes the biggest computational effort of the TPA.

In the helicopter under study, the vibro-acoustic TPA is performed considering the gearbox as the source and the cabin cavity as the receiver location. The gearbox is connected to the cabin

roof by means of two front struts, two rear struts and the anti-torque plate through four bolts leading to have eight structural paths. The transfer function matrix (equation 14) has been obtained by exciting the structure with an impact hammer and measuring the acceleration responses. The acceleration vector of equation 14 (i.e. $\left\{\ddot{X}_1 ... \ddot{X}_m\right\}^t$) has been calculated in flight operational conditions, so the operational forces can be calculated. Concerning equation 15, the vibro-acoustic transfer functions have been obtained taking advantage of the vibro-acoustic reciprocity (i.e. $p_i/F_j = -\ddot{X}_j/\dot{q}_i$, where $\dot{q}_i$ is the volume velocity at location j). Therefore the TFs have been calculated exciting by means of two volume acceleration sources working at different frequencies, 0 - 400 Hz and 400 - 4000 Hz, and measuring the responses using the accelerometers located in the eight structural paths. The sources were placed in the helicopter cabin, close to the pilot seat. Experimental data are used to implement a numerical TPA model. The model points out the most critical transfer paths and paves the way to a number of simulations that allows predicting the noise reduction achievable in the helicopter cabin for a given reduction of the source strength and as result of structural modifications. The analysis focused on the connecting points between the gearbox and the helicopters frame.

The spectral analysis of the computed operational loads combined with a spectral analysis of the sound pressure levels measured in the helicopter mock-up cabin during simulated operating conditions leads to the identification of a number of critical frequency tones that show a very efficient noise transmission mechanism in the helicopter cabin. Out of a list of critical frequencies, three main tones are hereby identified that are responsible for generating the largest contribution to the cabin noise spectrum. These tones correspond to the rotor shaft rotation and two of the gearbox meshing frequencies. The noise path analysis will then focus on those frequencies only. The analysis of the operational load spectra shows that the transmission path corresponding to the rear left and rear right struts and anti-torque plate exhibits the highest levels and provides the major contribution to the cabin noise at the identified critical frequencies. This means that any action aiming at reducing cabin noise recorded at those frequencies should focus on the anti-torque plate.

Once the main noise transmission paths contributing to the cabin noise are identified for the most critical noise frequency, the TPA model can be used to simulate the noise reduction that can be achieved if structural modifications would be implemented on the helicopter structure or on the gearbox in a process of noise control.

Two simulation scenarios are thus presented. One consists of introducing a modification in the TPA models; this can be easily done by editing the FRF of a selected transmission path and, e.g., zeroing the FRF amplitude in correspondence of the selected frequency. This is equivalent to simulating an active noise control system that induces a modification in the FRF of a specific transmission path. In order to select the best target frequency to be treated by the noise reduction simulation, a simple spectral analysis is carried out that shows the effect of zeroing the cumulatively the previously identified critical tones and compute the noise reduction that results from that action. In Tab. 3 it is shown that suppressing the two main gearbox meshing frequency tones for the most relevant transmission paths results into 5 dB(A) Sound Pressure Level (SPL) reduction as the SPL decreases from 111 dB(A) to 106 dB(A); yet suppressing the 5 highest tones results into 1 dB(A) more noise reduction (Tab. 3). Therefore, noise comfort improvement can be achieved with active control systems acting on the anti-torque plate hosting the gearbox. A second scenario consists of simulating a source modification that results into a frequency shift of a selected critical frequency. The considered source is the gearbox. The target frequency is again the meshing tone. This corresponds to simulate a design modification (gear diameter, number of teeth of a number of gears, etc) in

Original configuration	Suppression of the 2 main freq. tones	Suppression of the 5 main freq. tones	Shift of a meshing frequency in the gearbox
111 dB(A)	106 dB(A)	105 dB(A)	106 dB(A)

Table 3. Noise reduction cumulative effect after modifications of the TPA model.

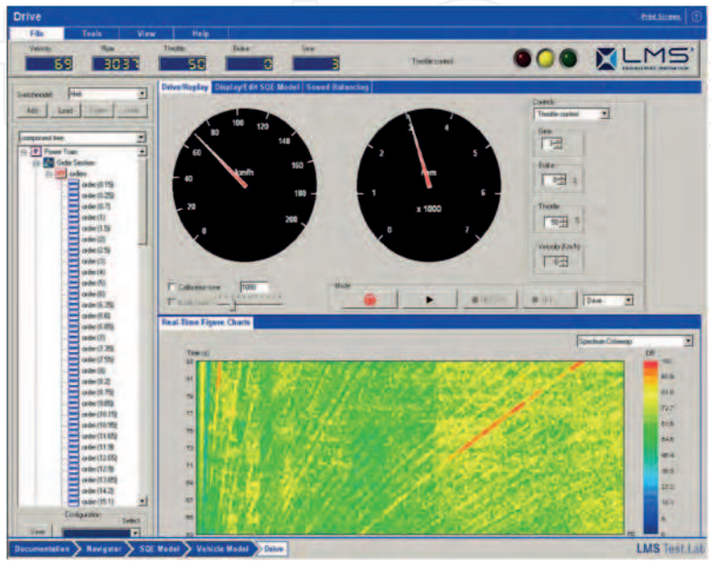

Fig. 21. Virtual Helicopter Sound Environment.

the gearbox resulting into a shift of the meshing frequency. The TPA model is then run again to compute a new set of partial pressure contributions to the interior cabin noise. 5 dB(A) reduction in the SPL can be observed.

6. Target sound design: The virtual helicopter sound environment

A sound synthesis approach was developed for helicopter noise (Vecchio et al., 2007). The noise synthesis is based on a compact and sound-quality-accurate model which is identified from measured noise data. A sound synthesis model consists of a number of tonal components and third octave bands that describe the broadband noise. The ground-reflection coefficient and the time-delay between the direct and reflected sound are also taken into account to characterize the typical interference pattern peculiar of flyover noise. For the few aircraft sounds studied so far, impressive synthesis results were achieved. Almost no differences could be heard between the synthesized and measured sounds. Acoustic engineers can easily modify model components and assess the impact on the human perception. This way they can design target sounds with improved sound quality and suggest guidelines for future design improvements. The sound synthesis helps better understand sound quality differences among various types of helicopters manoeuvres and forms an excellent basis to design target sounds with improved noise signature. A software environment (the Virtual Helicopter Sound Environment, see Figure 21) was developed where it is possible to virtually drive an helicopter and in the meantime, study the impact different modifications have on the noise perception and the sound quality. The tool was first designed for interior car sounds, but some modifications were implemented to cope with aircraft and helicopter noise.

Some of the tool's features are very relevant for the case under study: once the fundamental noise components have been suitably modelled, the sound can be synthesized and replayed according to any RPM evolution. Sound synthesis can then be recorded and stored on a data file. The advantage of the Virtual Helicopter Sound environment is here evident: one can easily modify model components and evaluate the impact on the human perception. A large variety of so-called "what if" scenarios can be played. For example, what happens if the dominant tonal components are reduced with 3 dB? Or what is the sound quality impact if the levels of some low or high frequency third octave noise bands are changed? Or what happens with our sensation of sharpness when the rapid amplitude variations of the high-frequency tonal components are smoothed? By playing some of these "what if" scenarios, one can design target sounds with improved sound quality and suggest engineering guidelines for noise control.

7. Concluding remarks

The work contributes to define a systematic experimental procedure aimed at identifying the noise sources, the mechanics of transfer from source to target (pilot and/or passenger area) and defining an effective noise control strategy in helicopters. This activity has led a number of conclusions:

1 Since the vibro-acoustical coupling between the cabin enclosure and the internal and external surfaces, is one of the cabin interior noise responsible, its assessment is necessary in a process of noise control;

2 Sound quality parameters and acoustics intensity analysis are effective tools for defining the relative importance of the noise produced by the jet engines with respect to the gearbox and for a fast and efficient localization of noise and vibration sources and leakage points in the helicopter cabin;

3 The TPA allows pointing out a subset of critical frequency tones that are transmitted into the helicopter cabin and a sub-set of transmission paths contributing the most to the cabin noise. The results show that noise comfort improvement can be achieved with active control systems acting on the anti-torque plate hosting the gearbox and with modifications of the meshing frequency in the gearbox;

4 The sound synthesis approach can be considered as an innovative technology, allowing engineers and designers to listen to their models and judge the sound quality impact of structural design modifications. This way they can design target sounds with improved sound quality and suggest guidelines for noise control.

8. References

M. Abdelghani, L. Hermans, H. Van der Auweraer (1999). A state space approach to output-only vibro-acoustical modal analysis, in: Proceedings of the 17th International Modal Analysis Conference, Vol. 3727, Kissimmee, FL, pp.1789-1793

A.T. Conlisk (2001). Modern helicopter aerodynamics, Progress in aerospace sciences, Vol. 37, pp. 419-476

H.E. De Bree, P. Leussink, T. Korthorst, H. Jansen, T. Lammerink, M. Elwenspoek (1996). The Microflown: a novel device measuring acoustical flows, Sensors and Actuators SNA054/1-3, pp. 552-557

H-E. de Bree, V.B. Svetovoy, R. Raangs, R. Visser (2004). "The very near field: Theory, simulations and measurements of sound pressure and particle velocity in the very near field", in: Proceedings of ICSV11, Eleventh International Congress on Sound and Vibration, St. Petersburg, Russia

W. Desmet, B. Pluymers, P. Sas (2003). Vibro-acoustic analysis procedures for the evaluation of the sound insulation characteristics of agricultural machinery cabins, Journal of Sound and Vibration 266, 407-441

G. C. Everstine (1997). Finite Element Formulations of structural acoustics problems, Computers and Structures 65, 307-321

G. C. Everstine (1981). Structural acoustic analogies for scalar field problems, International Journal of Numerical Methods in Engineering 17, 471-476

L.M. Gelman, D.A. Kripak, V.V. Fedorov, L.N. Udovenko (2000). Condition monitoring diagnosis methods of helicopter units, Mechanical system and signal processing, Vol. 14,No. 4, pp. 613-624

L. Hermans and H. Van der Auweraer (1999). Modal Testing and Analysis of Structures under Operational Conditions: Industrial Applications, Mechanical Systems and Signal Processing 13, 193-216

M. Kronast, M. Hildebrandt (2000). Vibro-acoustic modal analysis of automobile body cavity noise, Sound and Vibration 34. 20-23

Z.-D. Ma and I. Hagiwara (1991). Sensitivity analysis methods for coupled acoustical-structural systems. Part I: Modal sensitivities, AIAA J. 2, 1787–1795

E. Mucchi, A. Vecchio (2009). Experimental transfer path analysis on helicopters, Proceedings of the International Conference on Acoustics (NAG/DAGA2009), Rotterdam, Netherlands, 23-26 March, pp. 788-791

E. Mucchi, A. Vecchio (2010). Acoustical signature analysis of a helicopter cabin in steady-state and run up operational conditions, Measurement 43, 283-293

B. Peeters, H. Van der Auweraer, F. Vanhollebeke, P. Guillaume (2007). Operational modal analysis for estimating the dynamic properties of a stadium structure during a football game, Shock and Vibration – Special Issue: Assembly Structures under Crowd Dynamic Excitation 14, 283-303

E. Pierro, E. Mucchi, L. Soria, A. Vecchio (2009). On the vibro-acoustical operational modal analysis of a helicopter cabin - Mechanical Systems and Signal Processing, Volume 23, Issue 4, Pages 1205-1217

Pintelon, R., Schoukens, J. (2001). System Identification: a Frequency Domain Approach, New York: IEEE Press

A. Vecchio, C. Urbanet, F. Cenedese (2006). Experimental Noise Transfer Path Analysis on Helicopters, Proceedings of the International Conference on Noise and Vibration Engineering, 18-20 September, Leuven. Belgium

A. Vecchio, K. Janssens, C. Schram, J. Fromell, F. Cenedese (2007) Synthesis of Helicopters Flyover Noise for Sound Quality Analysis, Proceedings of the 13th AIAA/CEAS Aeroacoustics Conference, 21-23 May, Rome, Italy

Wallace, C.E. (1972). Radiation resistance of a rectangular panel, The Journal of the Acoustic Sociecy of America, Vol.51, N. 3, Part2

K. Wyckaert, F. Augusztinovicz, P. Sas (1996). Vibro-acoustical modal analysis: Reciprocity, model symmetry and model validity, Journal of Acoustical Society of America 100, 3172-3181

E. Zwicker, H. Fastl (1999). Psycho-acoustics, Facts and Models, Springer

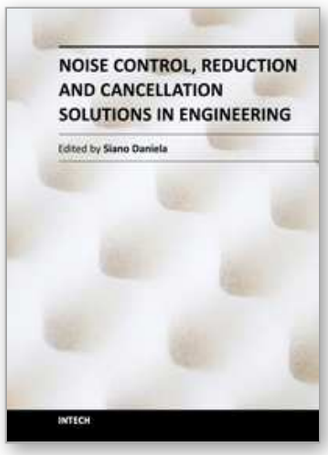

Noise Control, Reduction and Cancellation Solutions in Engineering

Edited by Dr Daniela Siano

ISBN 978-953-307-918-9
Hard cover, 298 pages
Publisher InTech
Published online 02, March, 2012
Published in print edition March, 2012

Noise has various effects on comfort, performance, and human health. For this reason, noise control plays an increasingly central role in the development of modern industrial and engineering applications. Nowadays, the noise control problem excites and attracts the attention of a great number of scientists in different disciplines. Indeed, noise control has a wide variety of applications in manufacturing, industrial operations, and consumer products. The main purpose of this book, organized in 13 chapters, is to present a comprehensive overview of recent advances in noise control and its applications in different research fields. The authors provide a range of practical applications of current and past noise control strategies in different real engineering problems. It is well addressed to researchers and engineers who have specific knowledge in acoustic problems. I would like to thank all the authors who accepted my invitation and agreed to share their work and experiences.

How to reference

In order to correctly reference this scholarly work, feel free to copy and paste the following:

Emiliano Mucchi, Elena Pierro and Antonio Vecchio (2012). Advanced Vibro-Acoustic Techniques for Noise Control in Helicopters, Noise Control, Reduction and Cancellation Solutions in Engineering, Dr Daniela Siano (Ed.), ISBN: 978-953-307-918-9, InTech, Available from: http://www.intechopen.com/books/noise-control-reduction-and-cancellation-solutions-in-engineering/advanced-vibro-acoustic-techniques-for-noise-control-in-helicopters

INTECH
open science | open minds

InTech Europe
University Campus STeP Ri
Slavka Krautzeka 83/A
51000 Rijeka, Croatia
Phone: +385 (51) 770 447
Fax: +385 (51) 686 166
www.intechopen.com

InTech China
Unit 405, Office Block, Hotel Equatorial Shanghai
No.65, Yan An Road (West), Shanghai, 200040, China
中国上海市延安西路65号上海国际贵都大饭店办公楼405单元
Phone: +86-21-62489820
Fax: +86-21-62489821

IntechOpen